

1 **WAVELET ANALYSIS OF THE SINGULAR SPECTRAL RECONSTRUCTED TIME SERIES TO STUDY**
2 **THE IMPRINTS OF SOLAR-ENSO-GEOMAGNETIC ACTIVITY ON INDIAN CLIMATE**

3
4 ¹S. Sri Lakshmi* and ²R. K. Tiwari

5
6 ¹ University Centre for Earth and Space Sciences, University of Hyderabad, Hyderabad 500 046,
7 India

8 ² CSIR-National Geophysical Research Institute, Uppal Road, Hyderabad 500 007, India
9

10 *Corresponding Author: srilakshmi.uceess@gmail.com

11 Tel.: +91-40-23132671 (Office)

12 Fax: +91-40-23010152
13

14 **ABSTRACT**

15 To study the imprints of the Solar-ENSO-Geomagnetic activity on the Indian Subcontinent, we
16 have applied the Singular spectral analysis (SSA) and wavelet analysis to the tree ring
17 temperature variability record from the Western Himalayas. Other data used in the present
18 study are the Solar Sunspot Number (SSN), Geomagnetic Indices (aa Index) and Southern
19 Oscillation Index (SOI) for the common time period of 1876-2000. Both SSA and wavelet
20 spectral analyses reveal the presence of 5-7 years short term ENSO variations and the 11 year
21 solar cycle indicating the possible combined influences of solar-geomagnetic activities and
22 ENSO on the Indian temperature. Another prominent signal corresponding to 33-year
23 periodicity in the tree ring record suggests the Sun-temperature variability link probably
24 induced by changes in the basic state of the earth's atmosphere. In order to complement the
25 above findings, we performed a wavelet analysis of SSA reconstructed time series, which agrees
26 well with our earlier results and increases the signal to noise ratio thereby showing strong
27 influence of solar-geomagnetic activity & ENSO throughout the entire period. The solar flares
28 are considered responsible for causing the atmospheric circulation patterns. The net effect of
29 solar-geomagnetic processes on the temperature record might suggest counteracting
30 influences on shorter (about 5–6 y) and longer (about 11–12 y) time scales. The present
31 analyses suggest that the influence of solar activities on the Indian temperature variability
32 operates in part indirectly through coupling of ENSO on multilateral time scales. The analyses,
33 hence, provide credible evidence for tele-connections of tropical pacific climatic variability and

34 Indian climate ranging from inter-annual-decadal time scales and also suggest the possible role
35 of exogenic triggering in reorganizing the global earth-ocean-atmospheric systems.

36 **Key words:** *Geomagnetic activity, Western Himalayas, Sunspot Number, SOI index, Singular*
37 *spectral analysis, Wavelet spectrum, Coherency.*

38

39 **1. Introduction:**

40 Several recent studies of solar/geomagnetic effects on climate have been examined on both
41 global as well as on regional scales (Lean and Rind, 2008; Benestaed and Schmidt, 2009; Meehl,
42 2009; Kiladis and Diaz 1989; Pant and Rupa Kumar 1997; Gray et al. 1992; Wiles et al. 1998; Friis
43 and Svensmark 1997; Rigozo et al. 2005; Feng et al. 2003; Tiwari and srilakshmi 2009; Chowdary
44 et al. 2006, 2014; Appenzeller et al. 1998; Proctor et al. 2002; Tsonis et al. 2005; Freitas and
45 Mclean 2013). The Sun's long-term magnetic variability caused by the sunspots is considered as
46 one of the primary drivers of climatic changes. The short-term magnetic variability is due to the
47 disturbances in Earth's magnetic fields caused by the solar activities and is indicated by the
48 geomagnetic indices. The Sun's magnetic variability modulates the magnetic and particulate
49 fluxes in the heliosphere. This determines the interplanetary conditions and imposes significant
50 electromagnetic forces and effects upon the planetary atmosphere. All these effects are due to
51 the changing solar-magnetic fields, which are relevant for planetary climates including the
52 climate of the Earth. The Sun-Earth relationship varies on different time scales ranging from
53 days to years bringing a drastic influence on the climatic patterns. The ultimate cause of solar
54 variability, at time scales from decadal to centennial to millennial or even longer scales has its
55 origin in the solar dynamo mechanism. During the solar maxima, huge amounts of solar energy
56 particles are released, thereby causing the geomagnetic disturbances. The 11 years solar cycle
57 acts as an important driving force for variations in the space weather, ultimately giving rise to
58 climatic changes. It is, therefore, imperative to understand the origin of space climate by
59 analyzing the different proxies of solar magnetic variabilities. Another important phenomenon
60 is El Nino-Southern Oscillation (ENSO), which associated with droughts, floods and intense
61 rainfall in different parts of the world. The strong coupling and interactions between the
62 Tropical Ocean and the atmosphere play a major role in the development of the global climatic

63 system. The El Nino events generally recur approximately every 3-5 years with large events
64 spaced around 3-7 years apart. The ENSO phenomena have shown huge impact on the Asian
65 monsoon (Cole et. al., 1993), Indian monsoon (Chowdary et al. 2006, 2014) as well as globally
66 (Horel and Wallace 1981; Barnett 1989; Yasunari 1985; Nicholson 1997). In particular, the El
67 Nino, solar, geomagnetic activities are the major affecting forces on the decadal and
68 interdecadal temperature variability on global and regional scales in a direct/indirect way (El-
69 Borie et al, 2010; Gray et al., 2010). Recent studies (Frohlich and Lean 2004; Steinhilber et al.
70 2009) indicate the possible influence of solar activity on Earth's temperature/climate on multi-
71 decadal time scales. The 11 year solar cyclic variations observed from the several temperature
72 climate records also suggest the impact of solar irradiance variability on terrestrial temperature
73 (Budyko 1969; Friis and Lassen 1991; Friis and Svensmark 1997; Kasatkina et al. 2007). The bi-
74 decadal (22 years) called the Hale cycle, is related to the reversal of the solar magnetic field
75 direction (Lean et al. 1995; Kasatkina et al. 2007). The 33 year cycle (Bruckener cycle) is also
76 caused by the solar origin, but it is a very rare cycle (Kasatkina et al. 2007). The 2–7 years ENSO
77 cyclic pattern and its possible coupling process is the major driving force for the temperature
78 variability (Gray et al. 1992; Wiles et al. 1998; Mokhov et al. 2000; Rigozo et al. 2007, Kothawale
79 et al. 2010). El-Borie and Al-Thoyaib, 2006; El-Borie et al., 2007 and El-Borie et al, 2010 have
80 indicated in their studies that the global temperature should lag the geomagnetic activity with a
81 maximum correlation when the temperature lags by 6 years. Mendoza et. al., 1991 reported on
82 possible connections between solar activity and El Nino's, while Reid and Gage (1988) and Reid
83 (1991) reported on the similarities between the 11-year running means of monthly sunspot
84 numbers and global sea surface temperature. These findings suggest that there is a possibility
85 of strong coupling between temperature-ENSO and solar-geomagnetic signals.

86 Several studies have been carried out to understand the climatic changes of India in the
87 past millennium using various proxy records e.g. ice cores, lake sediments, glacier fluctuations,
88 peat deposits etc. There is a lack of high-precision and high-resolution palaeo-climatic
89 information for longer time scale from the Indian subcontinent. Tree-ring data is a promising
90 proxy to retrieve high resolution past climatic changes from several geographical regions of
91 India (Bhattacharyya et al. 1988; Bhattacharyya et al. 1992; Hughes, 1992; Bhattacharyya and

92 Yadav, 1996; Borgaonkar et al. 1996; Chaudhary et al. 1999; Yadav et al. 1999; Bhattacharyya
93 and Chaudhary, 2003; Bhattacharyya et al. 2006; Shah et al. 2007) It has been noted that tree-
94 ring based climatic reconstructions in India generally do not exceed beyond 400 years records
95 except at some sites in the Northwest Himalaya. Thus, a long record of tree-ring data is needed
96 to extend available climate reconstruction further back to determine climatic variability on sub-
97 decadal, decadal and century scale. However, non-availability of older living trees in most of the
98 sites is hindering the preparation of long tree chronology. In a previous study (Tiwari and
99 Srilakshmi, 2009), we have studied the periodicities and non-stationary modes in the tree ring
100 temperature data from the same region (AD 1200-2000). To reveal significant connections
101 among the Solar-geomagnetic-ENSO 'triad' phenomena on tree ring width in detail for the
102 period from 1876-2000, we have applied here the Singular spectral analysis (SSA) and the
103 wavelet spectral analysis for Sunspot data, geomagnetic data (aa index), Troup Southern
104 Oscillation Index (SOI) and the Western Himalayas tree ring data. Here our main objective is to
105 employ wavelet-based analysis on SSA reconstructed time series to find out the evidence of the
106 possible linkages, if any, among ENSO-solar-geomagnetic in the Indian temperature records.

107

108 **2. Source and Nature of Data:**

109 The data analyzed here includes the time series of (1) Smoothed Sunspot number for solar
110 activity (2) Geomagnetic activity data (aa indices) (3) Troup Southern Oscillation Index (SOI) for
111 the study of El Nino-Southern Oscillation called ENSO (4) Western Himalayan temperature
112 variability record. All the data sets have been analyzed for the common period of 125 years
113 spanning over 1876-2000. The monthly sunspot number data has been obtained from the
114 Sunspot Index Data Center [http:// astro.oma.be/SIDC/](http://astro.oma.be/SIDC/). The Troup SOI data is obtained from the
115 Bureau of Meteorology of Australia, <http://www.bom.gov.au/climate/>. The data for
116 geomagnetic activity, aa Index, was provided by the National Geophysical Data Center, NGDC,
117 (<http://www.ngdc.noaa.gov/stp/GEOMAG/aastar.shtml>). The aa index is a measure of
118 disturbances level of Earth's magnetic field based on magnetometer observations at two, nearly
119 antipodal, stations in Australia and England. In recent studies, the tree ring proxy climate
120 indicators are being used for extracting information regarding past seasonal temperature or

121 precipitation/drought based on the measurements of annual ring width. The detailed
122 description of the data has been presented elsewhere (Yadav et. al., 2004). A brief account of
123 the data pertinent to the present analysis, however, is summarized here. The tree ring data
124 being analyzed here is one of the best temperature variability records (1876 to 2000) of the
125 pre-monsoon season in the Western Himalayas available. The mean temperature series is
126 obtained from nine weather stations including both from high and low elevation areas in the
127 Western Himalayas. Temperature variability history is based on widely spread pure Himalayan
128 cedar (*Cedrus deodara* (Roxb.) G. Don) trees and characterizes all the sites with almost no
129 ground vegetation and thereby minimizes individual variation in tree-ring sequences induced by
130 inter tree competition (Yadav et. al., 2004). The mean chronological structure is based on in
131 total 60 radii from 45 trees in total, statistical feature of which show that the chronology is
132 suitable for dendro-climatic studies back to AD 1226 (Yadav et. al., 2004).

133

134 **3. Methods applied:** To analyze the temporal series and to find the climatic structure, we have
135 here three methods: Principal component analysis (PCA), Singular Spectral analysis (SSA) and
136 wavelet analysis.

137 **3.1. Principal component analysis (PCA):** As a preliminary analysis, we have applied the
138 Principal component analysis (PCA) to the data sets for the reduction and extraction of
139 dimensionality of the data and to rate the amount of variation present in the original data set.
140 The purpose to apply the PCA is to identify patterns in the given time series. The new
141 components thereby obtained by the PCA analysis are termed as PC1, PC2, PC3 and so on, (for
142 the first, second and third principal components), and are uncorrelated. The different PCs
143 capture part of the variance and are ranked depending on their corresponding percentage
144 variance.

145

146 **3.2. Singular spectral analysis:** The Singular Spectrum Analysis (SSA) method is designed to
147 extract as much information as possible from a short, noisy time series without any prior
148 knowledge about the dynamics underlying the series (Broomhead and King, 1986; Vautard and
149 Ghil, 1989; Alonso et. al., 2005; Golyandina et al., 2001). The method is a form of principal

150 component analysis (PCA) applied to lag-correlations structures of the time series. The basic
 151 SSA decomposes an original time series into a new series which consists of trend, periodic or
 152 quasi-periodic and white noises according to the singular value decomposition (SVD) and
 153 provides the reconstructed components (RCs). The basic steps involved in SSA are:
 154 decomposition (involves embedding, singular value decomposition (SVD)) and reconstruction
 155 (involves grouping and diagonal averaging). Embedding decomposes the original time series
 156 into the trajectory matrix; SVD turns the trajectory matrix into the decomposed trajectory
 157 matrices. The reconstruction stage involves grouping to make subgroups of the decomposed
 158 trajectory matrices and diagonal averaging to reconstruct the new time series from the
 159 subgroups.

160 **Step1: Decomposition:**

161 **(a) Embedding:** The first step in the basic SSA algorithm is the embedding step where
 162 the initial time series change into the trajectory matrix. Let the time series be $Y = \{y_1, \dots, y_N\}$
 163 of length N without any missing values. Here the window length L is chosen such that $2 < L <$
 164 $N/2$ to embed the initial time series. We map the time series Y into the L lagged vectors, $Y_i =$
 165 $\{y_i, \dots, y_{i+L-1}\}$ for $i = 1, \dots, K$, where $K = N - L + 1$. The trajectory matrix T_Y ($L \times K$ dimensions) is

166 written as: $T_Y = \begin{pmatrix} Y_1 \\ Y_2 \\ \cdot \\ \cdot \\ Y_K \end{pmatrix} \dots\dots\dots(1)$

167 **(b) Singular Value Decomposition (SVD):** Here we apply SVD to the trajectory matrix T_Y
 168 to decompose and obtain $T_Y = UDV'$ called eigentriples; where U_i ($K \times L$ dimensions; $1 < i < L$) is an
 169 orthonormal matrix; D_i ($1 < i < L$) is a diagonal matrix of order L ; V_i ($L \times L$ dimensions; $1 < i < L$) is
 170 a square orthonormal matrix.

171 The trajectory matrix is thus written as $T_Y = \sum_{i=1}^d U_i \sqrt{\lambda_i} V_i^T$; $\dots\dots\dots(2)$

172 where the i^{th} Eigen triple of $T_i = U_i \times \sqrt{\lambda_i} \times V_i^T$, $i = 1, 2, 3, \dots, d$ in which $d = \max(i: \sqrt{\lambda_i} > 0)$.

173 **Step 2: Reconstruction:**

174 **(c) Grouping:** Here the matrix T_i is decomposed into subgroups according to the trend,
 175 periodic or quasi-periodic components and white noises. The grouping step of the
 176 reconstruction stage corresponds to the splitting of the elementary matrices T_i into several
 177 groups and summing the matrices within each group. Let $I = \{i_1, i_2, \dots, i_p\}$ be the group of indices
 178 i_1, \dots, i_p . Then the matrix T_I corresponding to the group I is defines as $T_I = T_{i_1} + T_{i_2} + \dots + T_{i_p}$. The split of
 179 the set of indices $J=1, 2, \dots, d$ into the disjoint subsets I_1, I_2, \dots, I_m corresponds to the equation
 180 (3):

$$181 \quad T = T_{I_1} + T_{I_2} + \dots + T_{I_m}. \quad \dots\dots\dots(3)$$

182 The sets I_1, \dots, I_m are called the eigen triple grouping.

183 **(d) Diagonal averaging:** The diagonal averaging transfers each matrix T into a time
 184 series, which is an additive component of the initial time series Y . If z_{ij} stands for a element
 185 matrix Z , the k th term of the resulting series is obtained by averaging z_{ij} over all i, j such that
 186 $i+j=k+2$. This is called diagonal averaging or the Hankelization of the matrix Z . The Hankel matrix
 187 HZ , is the trajectory matrix corresponding to the series obtained by the result of diagonal
 188 averaging.

189 Considering equation (3), let X ($L \times K$) matrix with elements x_{ij} , where $1 \leq i \leq L, 1 \leq j \leq K$.
 190 Here diagonal averaging transforms matrix X to a series g_0, \dots, g_{T-1} using the formula:

$$191 \quad g_k = \begin{cases} \frac{1}{k+1} \sum_{m=1}^{k+1} x_{m, k-m+2}^* & 0 \leq k < L^* - 1 \\ \frac{1}{L^*} \sum_{m=1}^{L^*} x_{m, k-m+2}^* & L^* - 1 \leq k < K^* \\ \frac{1}{T-k} \sum_{m=k-k^*+2}^{N-k+1} x_{m, k-m+2}^* & K^* - 1 \leq k < T \end{cases} \quad (4)$$

192 This diagonal averaging by equation (4) applied to the resultant matrix X_{I_n} , produces time series
 193 Y_n of length T . For such signal characteristics, it is essential to examine the time-frequency
 194 pattern as to understand whether a particular frequency is temporally consistent or
 195 inconsistent. Hence for non-stationary signals, we need a transform that will be useful to obtain
 196 the frequency content of the time series/signal as a function of time.

197 An alternative method for studying the non-stationarity of the time series is wavelet
 198 transform. For non-stationary signals, wavelets decomposition would be the most appropriate

199 method because the analyzing functions (the wavelets function) are localized both in time and
200 frequency.

201
202 **3.3. Wavelet spectral analysis:** During the past decades, wavelet analysis has become a popular
203 method for the analysis of aperiodic and quasi-periodic data (Grinsted et. al., 2004; Jevrejeva
204 et. al., 2003; Torrence and Compo, 1998; Torrence and Webster, 1999). In particular, it has
205 become an important tool for studying localized variations of power within a time series. By
206 decomposing a time series into time-frequency space, the dominant modes of variability and
207 their variation with respect to time can be identified. The wavelet transform has various
208 applications in geophysics, including tropical convection (Weng and Lau 1994), the El Niño–
209 Southern Oscillation (Gu and Philander 1995), etc. We have applied the wavelet analysis to
210 analyze the non-stationary signals which permits the identification of main periodicities of
211 ENSO-sunspot-geomagnetic in the time series. The results give us more insight information
212 about the evolution of these variables in frequency-time mode.

213 A wavelet transform requires the choice of analyzing function Ψ (called “mother
214 wavelet”) that has the specific property of time-frequency localization. The continuous wavelet
215 transform revolves around decomposing the time series into scaling components for identifying
216 oscillations occurring at fast (time) scale and other at slow scales. Mathematically, the
217 continuous wavelets transform of a time series $f(t)$ can be given as:

218
$$W_{\psi}(f)(a, b) = \frac{1}{\sqrt{a}} \int_{-\infty}^{\infty} f(t) \psi\left(\frac{t-b}{a}\right) dt \dots\dots\dots(5)$$

219 Here $f(t)$ represents time series, Ψ is the base wavelets function (here we have chosen the
220 Morlet function), with length that is much shorter than the time series $f(t)$. W stands for
221 wavelet coefficients. The variable ‘ a ’ is called the scaling parameter that determines the
222 frequency (or scale) so that varying ‘ a ’ gives rise to wavelet spectrum. The factor ‘ b ’ is related to
223 the shift of the analysis window in time so that varying b represents the sliding method of the
224 wavelet over $f(t)$.

225 In several recent analyses, complex Morlet wavelet has been found useful for
226 geophysical time series analysis. The Morlet is mostly used to find out areas where there is high

227 amplitude at certain frequencies. The complex Morlet wavelet can be represented by a periodic
 228 sinusoidal function with a Gaussian envelope and is excellent for Morlet wavelet may be
 229 defined mathematically, as follows:

$$230 \quad \psi(t) = \pi^{-1/4} e^{-i\omega_0 t} e^{-t^2/2} \dots\dots\dots(6)$$

231 where ω_0 is a non-dimensional value. ω_0 is chosen to be 5 to make the highest and lowest
 232 values of ψ approximately equal to 0.5, thus making the admissibility condition satisfied. The
 233 complex valued Morlet transform enables to extract information about the amplitude and
 234 phase of the signal to be analyzed. Wavelet transform preserves the self-similarity scaling
 235 property, which is the inherent characteristic feature of deterministic chaos. The continuous
 236 wavelet transform has edge artifacts because the wavelet is completely localized in time. The
 237 cone of influence (COI) is the area in which the wavelet power caused by a discontinuity at the
 238 edge has dropped to e^{-2} of the value to the edge. The statistical significance of the wavelet
 239 power can be assessed relative to the null hypotheses that the signal is generated by a
 240 stationary process with a given background power spectrum (P_k) of first order autoregressive
 241 (AR1) process. (Grinsted et. al., 2004)

$$242 \quad P_k = \frac{1 - \alpha^2}{|1 - \alpha e^{-2i\pi k}|^2} \dots\dots\dots(7)$$

243 where k is Fourier frequency index.

244 The cross wavelet transform is applied to two time series to identify the similar patterns
 245 which are difficult to assess from a continuous wavelet map. Cross wavelet power reveals areas
 246 with high common power. The cross wavelet of two time series x (t) and y (t) is defined as $W^{XY} =$
 247 $W^X W^{Y*}$, where * denotes complex conjugate. The cross wavelet power of two time series with
 248 background power spectra P_k^X and P_k^Y is given as

$$249 \quad D \left(\frac{|W_n^X(s) W_n^{Y*}(s)|}{\sigma_X \sigma_Y} < p \right) = \frac{Z_v(p)}{v} \sqrt{P_k^X P_k^Y}, \dots\dots\dots(8)$$

250 where $Z_v(p)$ is the confidence level associated with the probability p for a pdf defined by the
 251 square root of the product of the two χ^2 distributions (Torrence and Compo, 1998). The
 252 wavelet power is $|W_n^X(s)|^2$ and the complex argument of $|W_n^X(s)|$ can be interpreted as the local
 253 phase. The cross wavelet analysis gives the correlation between the two time series as function
 254 of period of the signal and its time evolution with a 95% confidence level contour. The
 255 statistical significance is estimated using red noise model.

256 Wavelet coherence is another important measure to assess how coherent the cross
 257 wavelet spectrum transform is in time frequency space. The wavelet coherence of two time
 258 series is defined as (Torrence and Webster, 1998)

$$259 \quad R_n^2(s) = \frac{|S(s^{-1} W_n^{XY}(s))|^2}{S(s^{-1} |W_n^X(s)|^2) \cdot S(s^{-1} |W_n^Y(s)|^2)} \dots\dots\dots(9)$$

260 where, S is a smoothing operator. The smoothing operator is written as $S(W) = S_{scale}(S_{time}$
 261 $(W_n(s)))$, where S_{scale} denotes smoothing along the wavelet scale axis and S_{time} smoothing in
 262 time. Here for the morelet wavelet, the smoothing operator is

$$263 \quad S_{time}(W)|_s = \left(W_n(s) * c_1 \frac{-t^2}{2s^2} \right) \dots\dots\dots(10)$$

$$264 \quad S_{time}(W)|_s = (W_n(s) * c_2 \Pi(0.6s))_n | \dots\dots\dots(11)$$

265 Where c_1 and c_2 are normalization constants and n is the rectangle function. The factor of 0.6 is
 266 empirically determined scale decorrelation length of the Morlet wavelet (Torrence and Compo,
 267 1998). The statistical significance level of the wavelet coherence is estimated using the Monte
 268 Carlo methods (Grinsted et. al., 2004).

269
 270 **4. Results and Discussion:**

271 We analyzed the data sets spanning over the period of 1876-2000 using the PCA, SSA and
 272 wavelet spectral analyses. Figure 1 shows four time series: (1) Smoothed Sunspot number
 273 representing solar activities; (2) Geomagnetic (aa indices); (3) Troup Southern Oscillation Index
 274 (SOI) for the study of ENSO and (4) Western Himalayan temperature variability record that are

275 analyzed in the present work. From visual inspection it is apparent from Fig. 1 that both WH
276 and SOI data show irregular and random pattern, while sunspot numbers have quasi- cyclic
277 character. Further WH tree ring record also exhibits distinct temperature variability but
278 nonstationary behavior at different scales. This variability might be suggestive of coupled global
279 ocean-atmospheric dynamics or some other factors, such as deforestation, anthropogenic, high
280 latitudinal influence etc (Yadav et. al., 2004).

281 **(Figure 1)**

282 Hence it is quite difficult to differentiate such a complex climate signals visually and difficult to
283 infer any clear oscillation without the help of powerful mathematical methods. For
284 identification of any oscillatory components and understanding the climatic variations on
285 regional and global scale, we have applied the PCA, SSA and wavelet analysis. Figure 2 shows
286 the principal components (PCs) for the first four eigen triples (PC1, PC2, PC3, PC4) for the given
287 data sets. Figure 3 shows the power spectra of the principal components (PCs) for the four data
288 sets shown in figure 2. From the figure 3, it is observed that the power spectra of PC1-4 for the
289 sunspot data exhibits high power at 124, 11, 4-2.8 years. The presence of high solar signal at
290 124 years indicates the quasi-stable oscillatory components in the data. The power spectra of
291 geomagnetic data also shows the presence of strong signals at 124, 10-11, 4-2 years suggesting
292 a strong link of solar-geomagnetic activity. The power spectra of WH temperature data shows
293 strong high power at ~62 years, 32-35 years, 11 years, 5 years and 2-3 years suggesting strong
294 combined influence of global ocean-atmospheric circulation, solar-geomagnetic and ENSO
295 effects on the Indian climate system. Climate cycles of 50-70 years have been widely reported
296 in various ocean and atmospheric phenomena (Ogurtsov, et al. 2002, Tiwari, 2005). Schiesinger
297 and Ramankutt (1994), Minobe (1997) have reported similar 55-70 year inter decadal
298 oscillations in global mean temperature. Dominant amplitudes corresponding to 62 and 32-35
299 years periodicities may, therefore, be linked to the Atlantic Multi-decadal Oscillation (AMO) of
300 ocean -atmospheric circulations. The 11-year peak is well known solar signal while the 2-5 year
301 periods apparently falls in ENSO frequency band. These results could be better confirmed by
302 applying the mathematical tools of SSA and wavelet analyses.

303 **(Figure 2 & 3)**

304 To explore the stationary characteristics of these peaks obtained by the PCA, we have applied
305 the Morlet based wavelet transform approach (Holschneider, 1995; Foufoula-Georgiou and
306 Kumar, 1995; Torrence and Compo, 1998; Grinsted et. al., 2004). The wavelet spectrum
307 identifies the main periodicities in the time series and helps to analyze the periodicities with
308 respect to time. Figure 4 shows the wavelet spectrum for the a) Smoothed Sunspot number for
309 solar activity (SSN) (b) Western Himalayan (WH) temperature variability record (c) Geomagnetic
310 activity and (c) Troup Southern Oscillation Index (SOI). From the wavelet spectrum of sunspot
311 time series (Figure 4a), the signal near 11-year is the strongest feature and is persistent during
312 the entire series indicating the non-stationary behavior of the sunspot time series. The wavelet
313 spectrum of SOI (figure 4c) shows strong amplitudes. However, due to non-stationary (time
314 variant) character of the time series, the observed spectral peaks (power) split in the interval of
315 2- 8 years. The wavelet power spectrum of the western Himalayan temperature variability
316 (Figure 4b) reveals significant power concentration at inter-annual time scales of 3-5 years and
317 at 11 years solar cycle. A dominant amplitude modes is also seen in the low frequency range at
318 around 35-40 years (at periods 1930-1980) corresponding to AMO cycles. Our result agrees well
319 with the results of other climate reconstructions (Mann et. al., 1995) from tree rings and other
320 proxies. The observed variability in AMO periodicity has also been reported in other tree ring
321 record (Gray et. al., 2004). The statistical significance of the wavelet power spectrum is tested
322 by a Monte Carlo method (Torrence and Compo, 1998). The WH spectra depicting statistically
323 significant powers above the 95% significance level at around 5 years, 11 years and 33 years
324 suggests possible imprint of sunspot-geomagnetic and ENSO phenomena on the tree ring data.
325 On shorter time scales, the wavelet power spectrum of the geomagnetic record (Fig. 4d) also
326 reveals statistically significant power at around 2, 4-8, 11 years period.

327 **(Figure 4)**

328 In order to have better visualization of similar periods in two time series and for the
329 interpretation of the results, cross wavelet spectrum has been applied. Figure 5 shows the cross
330 wavelet spectrum of the a) SSN-WH temperature data b) WH data-SOI and c) SSN-SOI data. The
331 contours (dark black lines) are the enclosing regions where wavelet cross power is significantly
332 higher, at 95% confidence levels. The wavelet cross-spectra of WH-SSN (Fig.5a) show

333 statistically significant high power over a period of 1895-1985 in 8-16 years band. It is seen that
334 the WH-SOI cross-spectra (Fig. 5b), the high power is observed at 2–4 year band and 8–16 years
335 as well. The SSN-SOI spectra (Fig. 5c) shows a strong correlation at 11 years solar cycle, which is
336 stronger during 1910-1950 and 1960-2000 (Rigozo et. al., 2002, Rigozo et. al., 2003) suggesting
337 the strongest El Nino and La Nina events indicating solar modulation on ENSO (Kodera, 2005;
338 Kryjov and Park, 2007). These results show a good correspondence in response of growth of the
339 tree ring time series during the intense solar activity. Hence the results strongly support the
340 possible origin of these periodicities from Solar and ENSO events. The interesting conclusion
341 from Fig. 5 is that WH–sunspot connections are strong at 11 years, ENSO–sunspot also exhibit
342 strong power around 11 years; the WH–ENSO connections are spread over three bands, the 2–4
343 y; 4–8 and 8–16 y, covering the solar cycle and its harmonics; the WH-geomagnetic exhibits
344 strong connections around 2-4, 4-6, 11 years and 35-40 years indicating the influence of solar-
345 geomagnetic activity on Indian temperature.

346 (Figure 5)

347
348 The Singular spectral analysis (SSA) is performed for all the four data sets with window length of
349 40. The SSA spectra with 40 singular values and its corresponding reconstructed series (varying
350 from RC1-15 in some cases) are plotted are shown in Figure 6 &7. The important insights from
351 SSA spectra are the identification of gaps in the eigen value spectra. As a rule, the pure noise
352 series produces a slowly decreasing sequence of singular values. The explicit plateau in the
353 spectra represents the ordinal numbers of paired eigen triples. The eigen triples 2-3 for the
354 sunspot data corresponds to 11 years period; eigen triples for 1-2,3-5,6-10,11-14 for the WH
355 temperature data are related to harmonic with specific periods (periods 33-35y, 11y, 5y, 2y);
356 eigen triples for 2-5,6-9,10-13 for the geomagnetic data are related to periods 11, 5,2 years.
357 The eigen triples for the SOI data represents to ~ 5-7, 2 years periods. In order to assess
358 periodicities, the periodogram and the wavelet power spectra are plotted using the SSA
359 reconstructed data (SSA-RC) (Figure 8). From the figure 8, the periodogram of SSA-RC of SSN
360 and Geomagnetic data shows strong power at ~120, 10-11 years; the SOI data shows strong
361 peaks at 6-9, 3, years & WH data shows strong power at ~32, ~10-11, 3-5 years. The wavelet

362 spectra for all the SSA-RC data confirms the results excepts for the periods at ~120 years, which
363 is beyond the maximum scaling period chosen for the present wavelet. The coherency plot of
364 the SSA-RC data sets (Figure 9) indicates a significant power at 33 years, 11 years, 2-7 years in
365 the WH temperature record suggesting the possible influences of Sunspot-geomagnetic activity
366 and ENSO through tele-connection and hence significant role of these remote internal
367 oscillations of the atmosphere-ocean system on the Indian climate system. Researchers have
368 attributed these phenomena to internal ocean dynamics and involve ocean atmospheric
369 coupling as well as variability in the strength of thermohaline circulations (Knight et. al., 2005;
370 Delworth and Mann, 2000).

371 **(Figures 6, 7, 8 & 9)**

372 In general our result agrees well with earlier findings in the sense that statistically
373 significant global cycles of coupled effects of Sunspot/geomagnetic and ENSO are present in the
374 land based temperature variability record. However, there are certain striking features in the
375 spectra that need to be emphasized regarding the western Himalayas temperature variability: i)
376 Inter-annual cycles in period range of 3-8 years corresponding to ENSO in the wavelet spectra
377 exhibit intermittent oscillatory characteristics throughout the large portion of the record (Fig 4);
378 ii) The 11 years solar cycle in the cross wavelet spectrum of SSN and SOI (Figure 5) indicate the
379 solar modulation in the ENSO phenomena (Kodera, 2005; Kryjov and Park, 2007). iii) The high
380 amplitude at 11 years in the time intervals 1900-1995 with a strong intensity from 1900-1995
381 shows a good correspondence with the high temperature variability for the interval of high
382 solar-geomagnetic activity. The Multi-decadal (30-40 years) periodicity identified here in
383 Western Himalayan tree ring temperature record matches with North Atlantic sea surface
384 temperature variability implying that the temperature variability in the western Himalayan is
385 not a regional phenomenon, but a globally tele-connected climate phenomena associated with
386 the global ocean-atmospheric dynamics system (Tiwari & srilakshmi, 2009; Delworth et. al.,
387 1993; Stocker, 1994). The coupled ocean-atmosphere system appears to transport energy from
388 the hot equatorial regions towards Himalayan territory in a cyclic manner. These results may
389 provide constraints for modeling of climatic variability over the Indian region and ENSO
390 phenomena associated with the redistribution of temperature variability. The solar-

391 geomagnetic effects play a major role in abnormal heating of the land surface thereby indirectly
392 affects the atmospheric temperature gradient between the land-ocean coupled systems. In the
393 present work, the connections between solar/geomagnetic activity and ENSO on the WH time
394 series are found to be statistically significant, especially when they are studied over contrasting
395 epochs of respectively high and low solar activity. The correlation plots for the SSA-RC data sets
396 of WH-sunspot, WH-aa index, WH-SOI and Sunspot-aa index are plotted in figure 10. It is
397 noticed that there is a correlation plots for the Geomagnetic-sunspot activity has a maximum
398 correlation value at 1 year lag suggesting the strong influence of sunspot & geomagnetic forcing
399 on one another. The cross-correlation plot for the WH data and the SOI represents a maximum
400 value at zero lag. The correlations plot for WH-sunspot & WH-geomagnetic index exhibits
401 almost the identical results suggesting the possible impact of solar activities on the Indian
402 temperature variability.

403 (Figures 10)

404 The net effect of solar activity on temperature record therefore appears to be the result
405 of cooperating or counteracting influences of earth's magnetic activity on the shorter and
406 longer periods, depending on the indices used; scale-interactions, therefore, appear to be
407 important. Nevertheless, the link between Indian climate and solar/geomagnetic activity
408 emerges as having the strong evidence; next is the ENSO-solar activity connection.

409

410 **5. Conclusions:**

411 In the present paper, we have studied and identified the periodic patterns from the published
412 Indian temperature variability records using the modern spectral methods of Singular spectral
413 analysis (SSA)-Wavelet methods. The application of wavelet analysis for the SSA reconstructed
414 time series, along with the removal of noise in the data identifies the existence of a high-
415 amplitude, recurrent, multi-decadal scale patterns that are present in Indian temperature
416 records. The power spectra of WH temperature data shows strong high power at ~62 years, 32-
417 35 years, 11 years, 5 years and 2-3 years suggesting a strong influence of solar-geomagnetic-
418 ENSO effects on the Indian climate system. The presence of dominant amplitude at 33-year
419 cycle periodicity corresponds to Atlantic Multidecadal Oscillation (AMO) cycles. It also suggests

420 the Sun-temperature variability probably involving the induced changes in the basic state of the
421 atmosphere. The 30-40 yrs periodicity in Western Himalayan tree ring temperature record
422 matches with the global signal of the coupled ocean-atmospheric oscillation (Delworth et. al.,
423 1993; Stocker, 1994) implying that the temperature variability in Himalayan is not a regional
424 phenomenon, but seems to be tele-connected phenomena with the global ocean-atmospheric
425 climate system. The coherency plots of the SSA reconstructed WH-Sunspot; WH-geomagnetic
426 and WH-SOI data sets show strong spectral signatures in the whole record confirming the
427 possible influences of Sunspot-geomagnetic activities and ENSO through teleconnection and
428 hence the significant role of these remote internal oscillations of the atmosphere-ocean system
429 on the Indian temperatures. We conclude that the signature of solar-geomagnetic activity
430 affects the surface air temperatures of Indian subcontinent. However, long data sets from the
431 different sites on the Indian continent are necessary to identify the influences of the 120 years
432 solar-geomagnetic cycles.

433

434 **Acknowledgements**

435 The authors are extremely thankful to the Editor Dr. Stéphane Vannitsem and the anonymous
436 reviewers for their professional comments, meticulous reading of the manuscript and valuable
437 suggestions to improve the manuscript. The authors thank Dr. Ram Ratan Yadav, Birbal Sahni
438 Institute of Palaeobotany, India for providing the Western Himalayan data. The authors
439 acknowledge Dr. Francisco Javier Alonso of University of Extremadura for using the SSA routine
440 in a MATLAB environment. We are thankful to Dr. Grinsted and his colleagues for providing the
441 wavelet software package. First author acknowledged the Head, University Centre for Earth &
442 Space Sciences, University of Hyderabad for providing the facilities to carry out this work. RKT is
443 grateful to DAE for RRF.

444

445 **References**

446 Alonso, F. J., Castillo, J., and Pintado, P. (2005), "Application of Singular Spectrum Analysis to the
447 Smoothing of Raw Kinematic Signals," *Journal of Biomechanics*, 38(5), 1085–1092.

448 Appenzeller, C., Stocker, T. F., and Anklin, M. (1998). North Atlantic Oscillation Dynamics Record in
449 Greenland Ice Cores. *Science*, 282(5388), 446–449.

450 Barnett, T.P., et al. (1989). The effect of Eurasian snow cover on regional and global climate
451 variations. *J. Atmos. Sci.*, 48, 661–685.

452 Benestaed, R.E., and Schmidt, G.A., (2009), Solar trends and global warming, *Journal of Geophysical*
453 *research*, P 114.

454 Bhattacharyya A, LaMarche VC, and Telewski FW, (1988) Dendrochronological reconnaissance of the
455 conifers of Northwest India, *Tree-Ring Bull.*, 48: 21-30.

456 Bhattacharyya A, and Chaudhary V, (2003) Late-summer temperature reconstruction of the Eastern
457 Himalayan Region based on tree-ring data of *Abies densa*, *Arct. Antarct. Alp.Res.*, 35(2): 196-202.

458 Bhattacharyya A, and Yadav RR, (1996) Dendrochronological reconnaissance of *Pinus wallichiana* to
459 study glacial behaviour in the western Himalaya. *Current Science*, 70 (8): 739-744.

460 Bhattacharyya A, Shah, Santosh K, and Chaudhary V, (2006) Would tree-ring data of *Betula utilis* be
461 potential for the analysis of Himalayan Glacial fluctuations?, *Current Science*, 91(6): 754-761.

462 Bhattacharyya A, Yadav RR, Borgaonkar HP, & Pant GB, (1992) Growth ring analysis of Indian tropical
463 trees: Dendroclimatic potential, *Current Science*, 62: 736-741.

464 Bhattacharyya, A. and Yadav, R.R., (1992) Tree growth and recent climatic changes in the western
465 Himalaya, *Geophytology*, 22, 255-260.

466 Bigg GR, (1996) *The oceans and Climate*, Cambridge University Press, Cambridge, 1-266.

467 Borgaonkar HP, Pant GB, & Rupa Kumar k, (1996) Ring width variations in *Cedrus deodara* and its
468 climatic response over the Western Himalaya. *Intern. J. Climatol.* 16: 1409-1422.

469 Broomhead, D.S., and King, G.P., (1986). Extracting qualitative dynamics from experimental data,
470 *Physica D* 20, 217–236.

471 Budyko, M. I. (1969). The effect of solar radiation variations on the climate of the Earth. *Tellus*, 21,
472 611–619

473 Cane MA, (1992) Tropical Pacific ENSO models: ENSO as a mode of the coupled system. In: *Climate*
474 *System Modelling*, Ed: K.E. Trenberth, Cambridge University Press, Cambridge, 583-614.

475 Chaudhary V, Bhattacharyya A, and Yadav RR, (1999) Tree-ring studies in the Eastern Himalayan
476 region: Prospects and problems, *IAWA*, .20(3): 317-324.

477 Chowdary, J. S., John, N., and Gnanseelan, C. (2014). Interannual variability of surface air-
478 temperature over India: impact of ENSO and Indian Ocean Sea surface temperature. *Int. J.*
479 *Climatol.*, 34, 416–429.

480 Chowdary, J.S., Gnanseelan, C., Vaid, B.H., and Salvekar, P.S. (2006). Changing trends in the tropical
481 Indian Ocean SST during La Nina years. *Geophys. Res. Lett.*, 33, L18610. doi:10.1029/
482 2006GL026707.

483 Cole JE, Fairbanks RG, and Shen GT, (1993) Recent variability in the Southern Oscillation: Isotopic
484 results from a Tarawa Atoll coral. *Science*, 260: 1790-1793.

485 De Freitas, C., and Mclean, J. (2013). Update of the Chronology of Natural Signals in the Near Surface
486 Mean Global Temperature Record and the Southern Oscillation Index. *International Journal of*
487 *Geosciences*, 4 (1), 234–239.

488 Delworth T, and Mann M, (2000) Observed and Stimulated multidecadal variability in the Northern
489 Hemisphere, 16: 661-676.

490 Delworth T, Manabe S & Stouffer RJ (1993) Interdecadal variations of the thermohaline circulation in
491 a coupled ocean-atmosphere model. *J. Climate* 6: 1991-2011.

492 El-Borie, M.A., Shafik, E., Abdel-Halim, A.A., El-Monier, S., (2010), Spectral analysis of solar
493 variability and their possible role on the global warming (1880-2008), *Journal of Enviromental*
494 *Protection*, 1, pp 111-120.

495 El-Borie, M.A., Al. Thoyaib, S.S, Al-Sayed, N., (2007), *The 2nd Inter. CPMS*, 302.

496 El-Borie, M.A., and Al-Thoyaib, S.S., (2006), Can we use the aa geomagnetic activity index to predict
497 partially the variability in global mean temperature, *Journal of Physical Sci.*,1(2), pp 67–74.

498 Feng, S.H., Kaufman, D., Yoneji, S., Nelson, D., Shemesh, A., Huang, Y., Tian, J., Bond, G., Benjamin, C.,
499 and Brown, T. (2003). Cyclic Variation and Solar Forcing of Holocene Climate in the Alaskan
500 Subarctic. *Science*, 301, 1890–1893.

501 Foufoula-Georgiou E, and Kumar P, (Eds.), (1995) *Wavelets in Geophysics*, Academic San Diego, Calif.,
502 373pp.

503 Friis, C.E., and Lassen, K. (1991). Length of the Solar Cycle: An Indicator of Solar Activity Closely
504 Associated with Climate. *Science*, 254 (5032), 698–700.

505 Friis, C.E., and Svensmark, H. (1997). What do we really know about the sun- climate connection?,
506 Adv. Space Res., 20, 415, 913–9211.

507 Frohlich, C., and Lean, J. (2004). Solar radiative output and its Variability: Evidence and Mechanisms.
508 The Astron Astropys Rev., 12, 273–320.

509 Golyandina, N., Nekrutkin, V. V., and Zhigljavski, A. A. (2001), Analysis of Time Series Structure:
510 SSA and Related Techniques, Boca Raton: CRC Press.

511 Gray L.J., Beer, J., Geller, M., Haigh, J.D., Lockwood, M., Matthes, K., Cubasch, U., Fleitmann, D.,
512 Harrison, G., Hood, L., Luterbacher, J., Meehl, G.A., Shindell, D., van Geel B., and White, W., (2010).
513 Solar influences on climate, Reviews of Geophysics, 48, RG 4001, doi: 10.1029/2009RG000282.

514 Gray ST, Graumlich LJ, Betancourt JL, and Pederson GT, (2004) A tree-ring based reconstruction of the
515 Atlantic Multidecadal Oscillation since 1567 A.D, Geophys. Res. Lett. , 31: L12205,
516 doi:10.1029/2004GL019932.

517 Gray, W. M., Sheaffer, J. D., and Knaff, J. A. (1992). Hypothesized mechanism for stratospheric QBO
518 influence on ENSO variability. Geophys. Res. Lett., 19, 107–110.

519 Grinsted A, Moore JC, Jevrejeva S (2004) Application of the cross wavelet transform and wavelet
520 coherence to geophysical time series, Nonlin. Processes Geophys., 11: 561–566,
521 doi:10.5194/npg-11-561-2004

522 Gu, D., and Philander, S.G.H., (1995). Secular changes of annual and inter-annual variability in the
523 tropics during the past century, J. Clim. 8, 64–876.

524 Holschneider M (1995) Wavelets: An Analysis Tool, Oxford University Press, New York, 455.

525 Horel, J.D., and Wallace, J.M. (1981). Planetary-scale atmospheric Phenomena associated with the
526 Southern Oscillation, Monthly weather review, 109, 813-829.

527 Hughes MK (1992) Dendroclimatic evidence from the Western Himalaya. In: R.S. Bradley &
528 D. Jones (eds.), Climates since AD 1500: 4 15-431. Routledge. London.

529 Jevrejeva S, Moore JC, Grinsted A (2003) Influence of the Arctic Oscillation and El Niño-Southern
530 Oscillation (ENSO) on ice conditions in the Baltic Sea: The wavelet approach, J. Geophys. Res.,
531 108(D21), 4677, doi:10.1029/2003JD003417.

532 Ji JF, Shen J, Balsam W, Chen J, Liu L & Liu XQ, (2005) Asian monsoon oscillations in the northeastern
533 Qinghai-Tibet Plateau since the late glacial as interpreted from visible reflectance of Qinghai Lake
534 sediments, *Earth and Planetary Science letters* 233: 61-70.

535 Kasatkina, E.A., Shumilov, O.I., and Krapiec, M.(2007). On periodicities in long term climatic variations
536 near 68_N, 30_E. *Adv. Geosci*, 13, 25–29.

537 Kiladis, G.N., and Diaz, F.H. (1989). Global Climatic Anomalies Associated with Extremes in the
538 Southern Oscillation. *J. Climate*, 2, 1069–1090.

539 Knight JR, Allan RJ, Folland CK, Vellinga M, and Mann ME, (2005) A signature of persistent natural
540 thermohaline circulation cycles in observed climate'. *Geophys. Res. Lett.*, 32, L20708,
541 doi:10.1029/2005GL024233.

542 Kodera, K., and Y.Kuroda (2005). A possible mechanism of the spatial structure of the North Atlantic
543 Oscillation, *Journal of Geophysics Research*, 110, D02111, doi: 10.1029/2004JD005258.

544 Kothwale, D.R., Munot, A.A., and Krishna Kumar, K. (2010). Surface air temperature variability over
545 India during 1901-2007 and its association with ENSO. *Climate Research*, 42, 89–104,
546 doi:10.3354/cr00857.

547 Kryjov, V.N., and Park, Chung-Kyu, (2007). Solar modulation of the El-Nino/Southern Oscillation
548 impact on the Northern Hemisphere annular mode, *Geophysical research letters*, Vol. 34,
549 L10701, doi: 10.1029/2006GL028015.

550 Lean, J.L. and Rind, D.H., (2008), How natural and anthropogenic influences alter global and
551 regional surface temperatures: 1889 to 2006, *Journal of Geophysical Research*, Letter, p 35.

552 Lean, J., Beer, J., and Bradley, R. (1995). Reconstruction of solar irradiance since 1610: Implications
553 for climate change. *Geophy. Res.Lett.*, 22, 3195-3198.

554 Mann ME, Park J, and Bradley RS, (1995) Global interdecadal and century-scale climate oscillations
555 during the past 5 centuries, *Nature*, 378: 266–27.

556 Meehl, G.A., Arblaster, J.M., Matthes, K., Sassi, F., and Van Loon, H. (2009). Amplifying the Pacific
557 climate system response to a small 11-year solar cycle forcing. *Science*, 325, 1114–1118.

558 Mendoza B, Perez-Enriquez R, and Alvarez-Madrigal M, (1991) Analysis of solar activity conditions
559 during periods of El Nino events, *Ann. Geophysicae*, 9: 50-54.

- 560 Minobe, S. (1997). A 50-70 year climatic oscillation over the North Pacific and North
561 America. *Geophysical Research Letters*, 24(6), 683-686.
- 562 Mokhov, I. I., Eliseev, A.V., Handorf, D., Petukhov, V.K., Dethloff, K., Weishierner, A., and
563 Khvorostyanov, D. V. (2000). North Atlantic Oscillation: Diagnosis and simulation of decadal
564 variability and its long period evolution. *Atmospheric and Ocean physics*, 36, 555–565.
- 565 Nicolson, S. E. (1997). An analysis of the Enso signal in the tropical Atlantic and western Indian
566 oceans. *Int. J. Climatol.*, 17, 345–375.
- 567 Ogurtsov, M. G., Nagovitsyn, Y. A., Kocharov, G. E., & Jungner, H. (2002). Long-period cycles of
568 the Sun's activity recorded in direct solar data and proxies. *Solar Physics*, 211(1-2), 371-
569 394.
- 570 Pant, G.B., and Rupa Kumar, K. (1997). *Climates of South Asia*. John Wiley and Sons, Chichester, 320
571 pp.
- 572 Philander SG, (1990) *El Nino, La Nina and the Southern Oscillation*. Academic Press, London, 1-293.
- 573 Proctor, C.J., Baker, A., and Barnes, W. L. (2002). A three thousand year record of North Atlantic
574 Climate. *Clim.Dyn*, 19, 449–454.
- 575 Reid GC and Gage KS, (1988) The climatic impact of secular variations in solar irradiance, in *Secular*
576 *Solar and geomagnetic Variations in the Last 10000 years'*, Eds. F.R. and A.W. Wplfendale, NATO
577 AS Series, Kluwer, Dordrecht, 225-243.
- 578 Reid GC, (1991) Solar irradiance variations and global Ocean Temperature, *Journal of Geomagn.*
579 *Geoelectr.*, 43: 795-801.
- 580 Rigozo NR, Noredmann DJR, Echer E, Zanandrea A, Gonzalez WD, (2002) Solar variability effects
581 studied by tree-ring data wavelet analysis, *Adv. Space Res.*, 29(12): 1985-1988.
- 582 Rigozo NR, Vieira Lea, Echer E, Nordemann DJR, (2003) Wavelet analysis of Solar-ENSO imprints in
583 tree-ring data from Southern Brazil in the last century, *Climatic change*, 60: 329-340.
- 584 Rigozo, N. R., Nordeman, D. J. R., Echer, E., Vieira, L. E. A., Echer M. P. S. and Presets, A.(2005). Tree-
585 ring width wavelet and spectral analysis of solar variability and climatic effects on a Chilean
586 cypress during the last two and a half millennia. *Climate of the Past Discussions*, 1, 121–135.
- 587 Rigozo, N. R., Nordeman, D.J.R., Silva, H.E., Echer, M.P.S. and Echer, E. (2007). Solar and climate signal
588 records in tree ring width from Chile (AD1587–1994). *Planetary and Space Science*, 55, 158–164.

589 Shah Santosh K, Bhattacharyya A, and Chaudhary V, (2007) Reconstruction of June-September
590 Precipitation based on tree-ring data of Teak (*Tectona grandis* L.) from Hoshangabad, Madhya
591 Pradesh, India. *Dendrochronologia*, 25: 57-64.

592 Schlesinger, M E and Ramankutti, N, 1994, An oscillation in the global climate system of period 65-70
593 years. *Nature*, vol 367, pp723-726

594 Steinhilber, F., Beer, J. and Frohlich, C. (2009). Total solar irradiance during the Holocene. *Geophys.*
595 *Res. Lett.*, 36, L19704.

596 Stocker TF (1994). The variable ocean. *Nature* 367: 221-222.

597 Tiwari RK, and Srilakshmi S, (2009). Periodicities and non-stationary modes in tree ring temperature
598 variability record of the Western Himalayas by multitaper and wavelet spectral analyses, *Current*
599 *Science*, 97, 5: 705-709.

600 Tiwari (2005). *Geospectroscopy*, Capital Publ Co, New Delhi. Page 308.

601 Torrence C, Compo GP, (1998). A practical guide to wavelet analysis, *Bull. Am. Meteorol. Soc.*, 79: 61–
602 78

603 Torrence C, Webster P, (1999). Interdecadal changes in the ENSO-Monsoon System, *J.Clim.*, 12:
604 2679–2690.

605 Trenberth K, and Hoar TJ, (1997). El Nino and climate change. *Geophys. Res. Lett.*, 24: 3057–3060.

606 Tsonis, A. A., Elsner, J. B., Hunt, A. G., and Jagger, T. H. (2005). Unfolding the relation between global
607 temperature and ENSO. *Geophys. Res. Lett.*, 32, L09701.

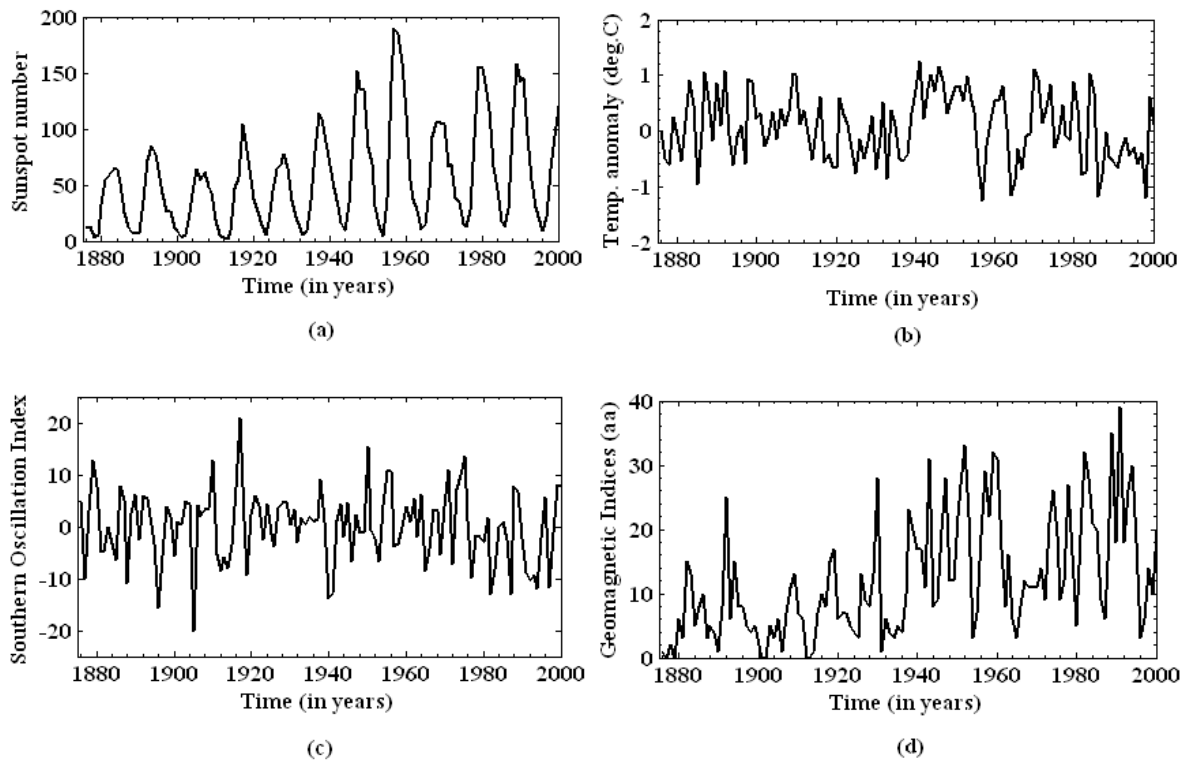
608 Vautard, R., and Ghil, M. (1989). Singular spectrum analysis in nonlinear dynamics, with applications
609 to paleoclimatic time series. *Phys. D*, 35, 395–424.

610 Weng, H., and K.-M. Lau, 1994: Wavelets, period doubling, and time-frequency localization with
611 application to organization of convection over the tropical western Pacific. *J. Atmos. Sci.*, 51,
612 2523–2541.

613 Wiles, G. C., D'Arrigo, R. D., and Jacoby, G. C. (1998). Gulf of Alaska atmosphere-ocean variability over
614 recent centuries inferred from coastal tree-ring records, *Climatic Change*, 38,

615 Yadav RR, Park WK, and Bhattacharyya A, (1999) Spring-temperature variations in western Himalaya,
616 India, as reconstructed from tree-rings: AD 1390-1987, *The Holocene*, 9(1): 85-90.

617 Yadav RR, Park WK, Singh J & Dubey B, (2004) Do the western Himalayas defy global warming?',
618 Geophysical Research Letters 31: L17201, doi: 10.1029/2004GL020201.
619 Yasunari, T. (1985). Zonally propagating modes of the global east–west circulation associated with
620 the Southern Oscillation. *J. Meteorol. Soc. J.*, 63, 1013–1029.
621
622
623
624
625
626
627
628
629
630
631
632
633

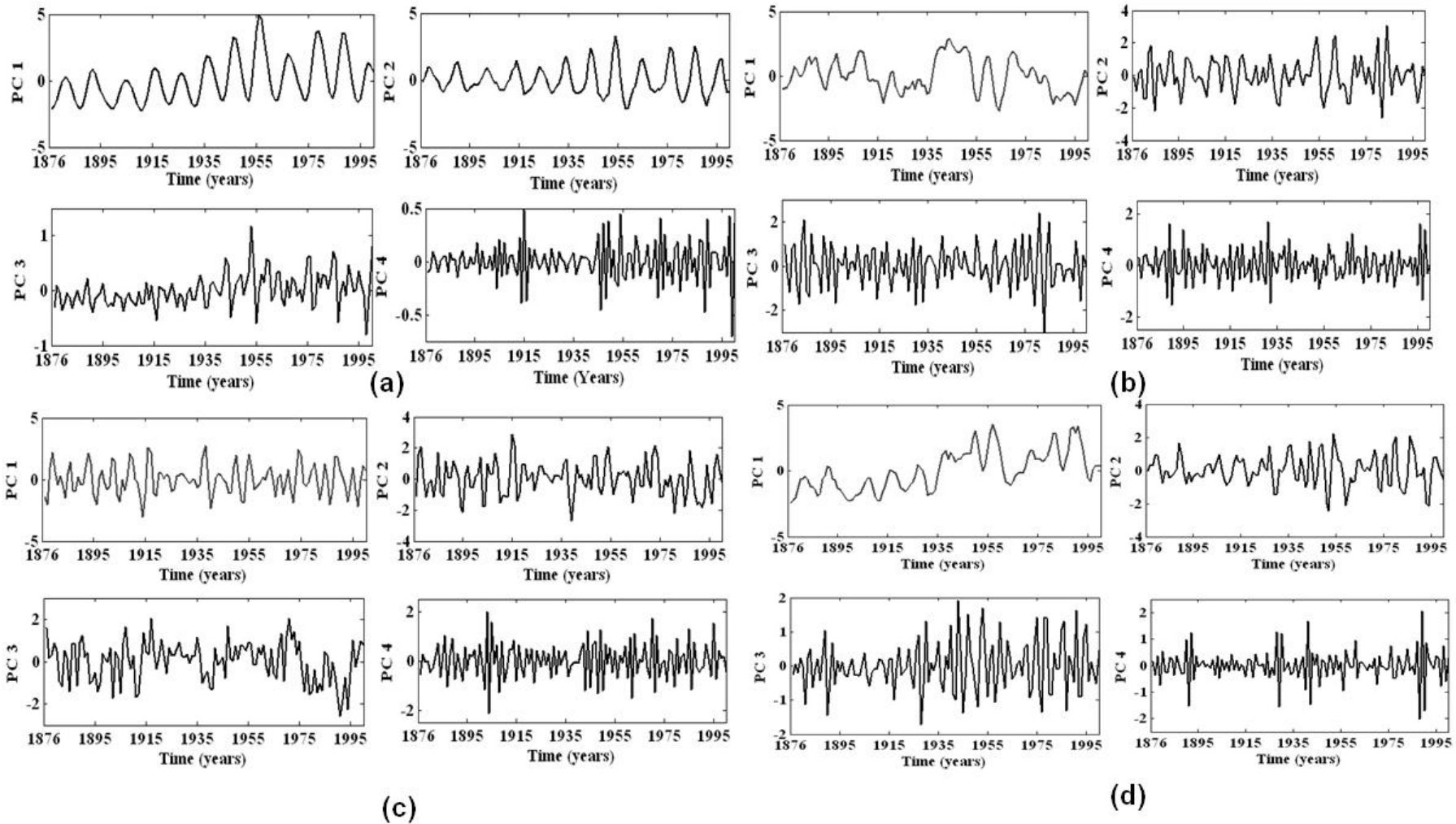


634

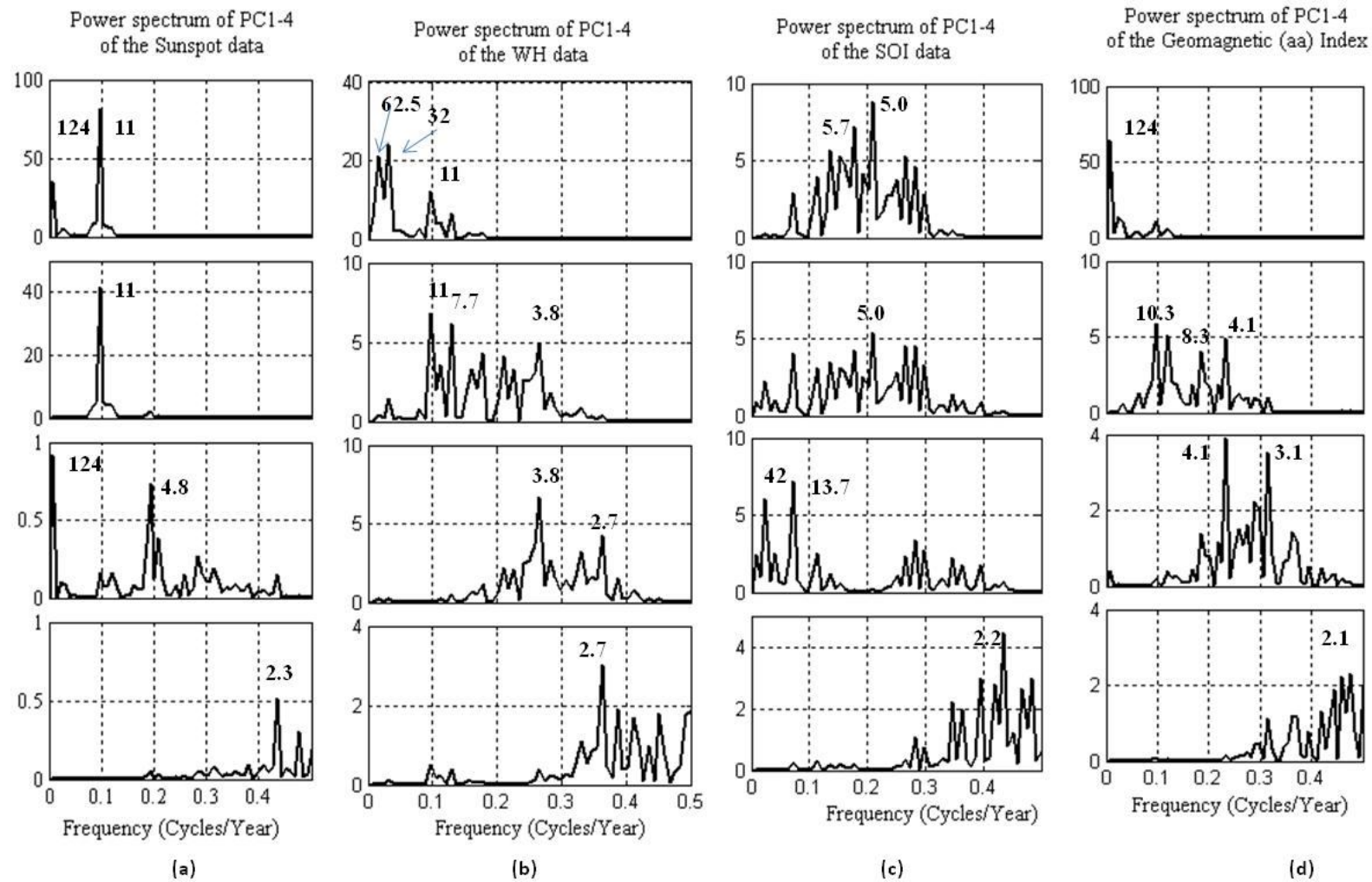
635 **Figure 1. Time series data of (a) Sunspot Index (b) the mean pre-monsoon temperature**
 636 **anomalies of the Western Himalayas (Yadav et. al., 2004) (c) Southern Oscillation Index**
 637 **(SOI) and (d) Geomagnetic Indices (aa indices) for common period 1876-2000.**

638

639

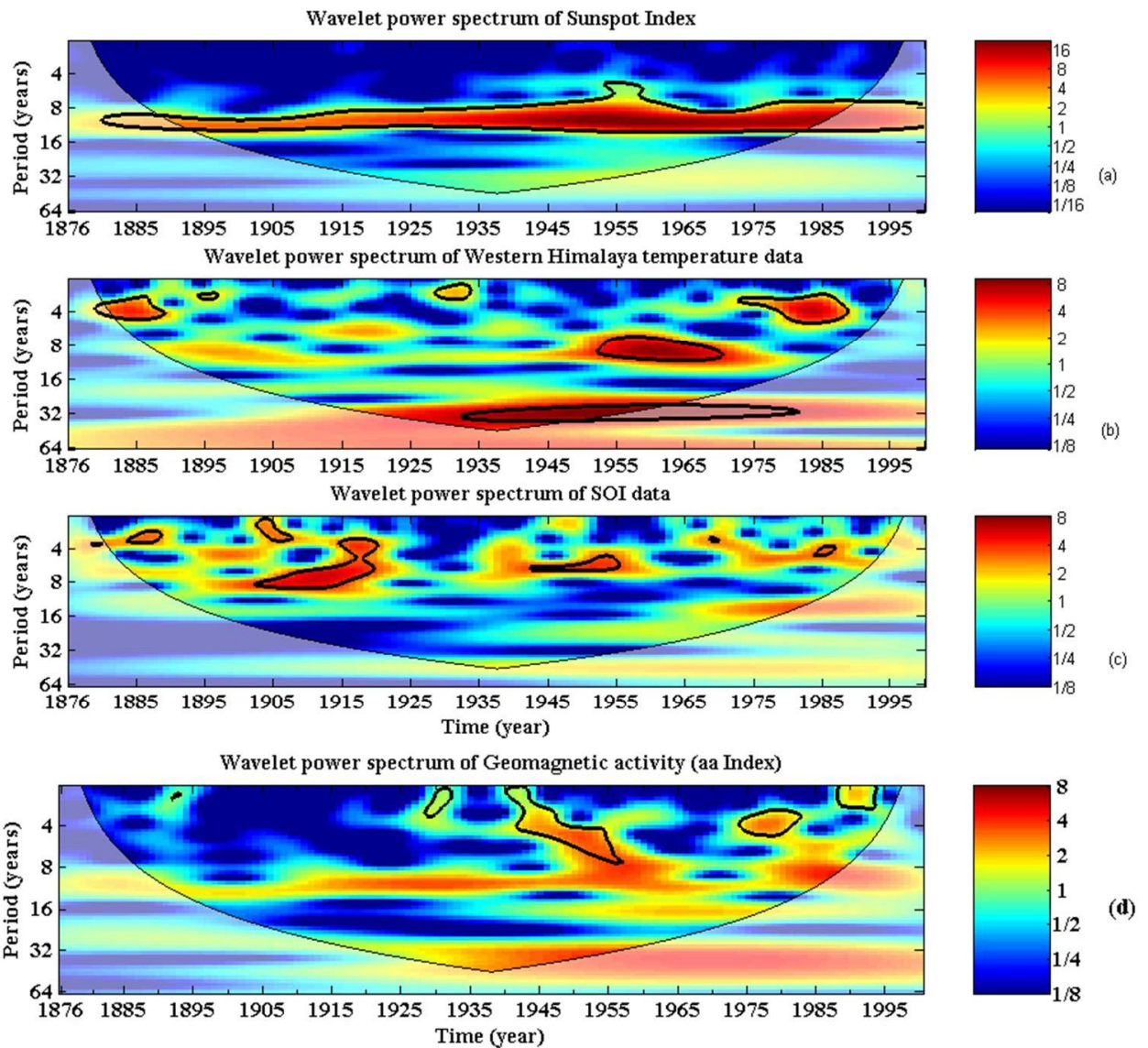


640
 641 **Figure 2. First four principal components (PCs:1-4) for time series (a) Sunspot numbers (b) the mean pre-monsoon temperature anomalies**
 642 **of the Western Himalayas (c) SOI index and (d) Geomagnetic Indices (aa indices) for the period 1876-2000.**



643

644 Figure 3. Power spectra of the first four principal component (PCs) (PC1-4 shown in Fig. 2) for all the data sets with their significant
 645 periodicities at 124, 11, 4 and 2.8 years are indicated in bold letters.

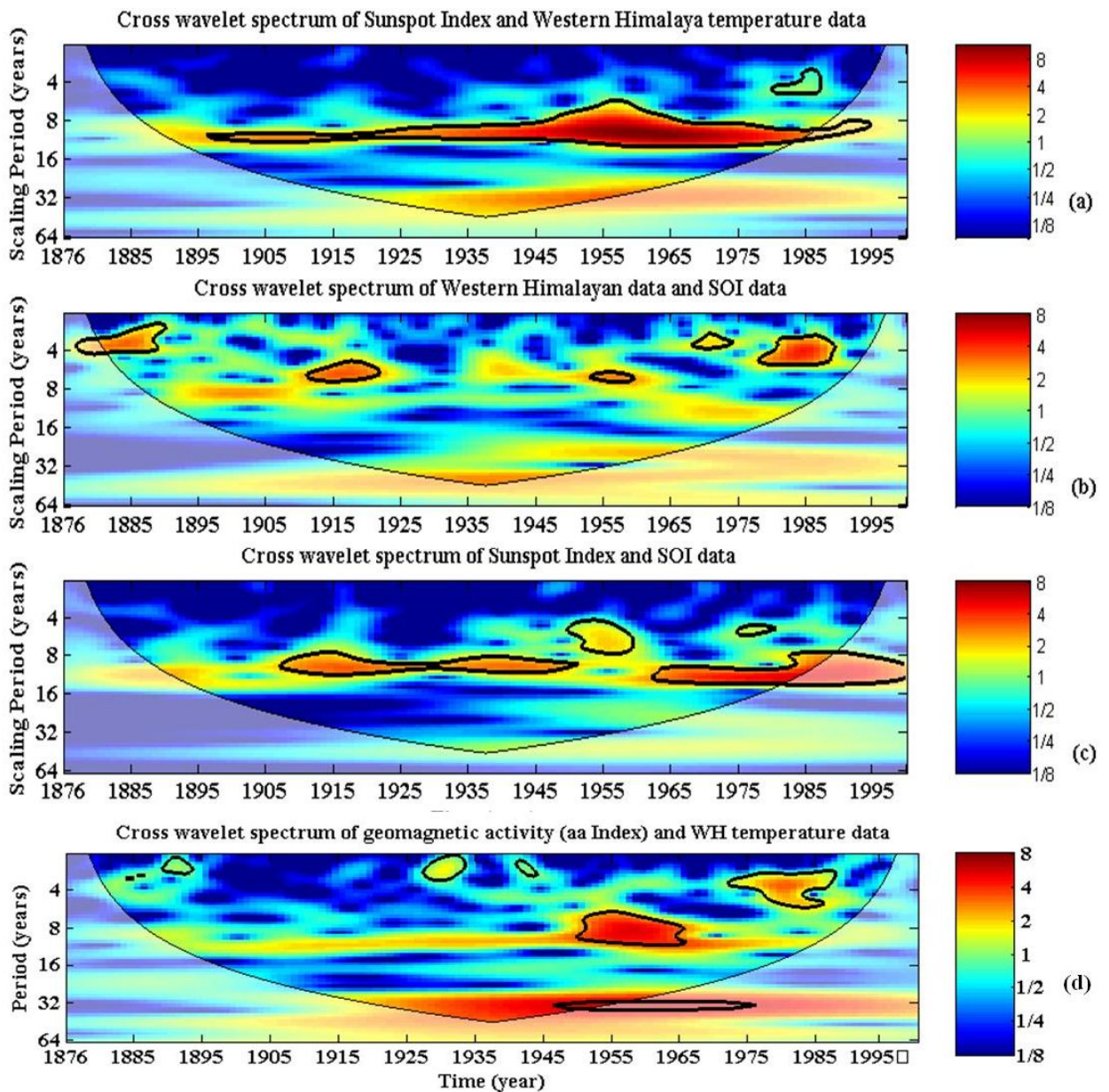


646

647 **Figure 4. Wavelet power spectrum of (a) Sunspot Number (b) Western Himalaya temperature**
 648 **data (c) Southern Oscillation Index (SOI) and (d) Geomagnetic activity (aa Indices) with cone**
 649 **of influence (lighter shade smooth curve) and black lines indicate significant power on 95%**
 650 **level compared to red noise based on first order auto-regressive (AR(1)) coefficient. The**
 651 **legend on right indicates the cross-wavelet power.**

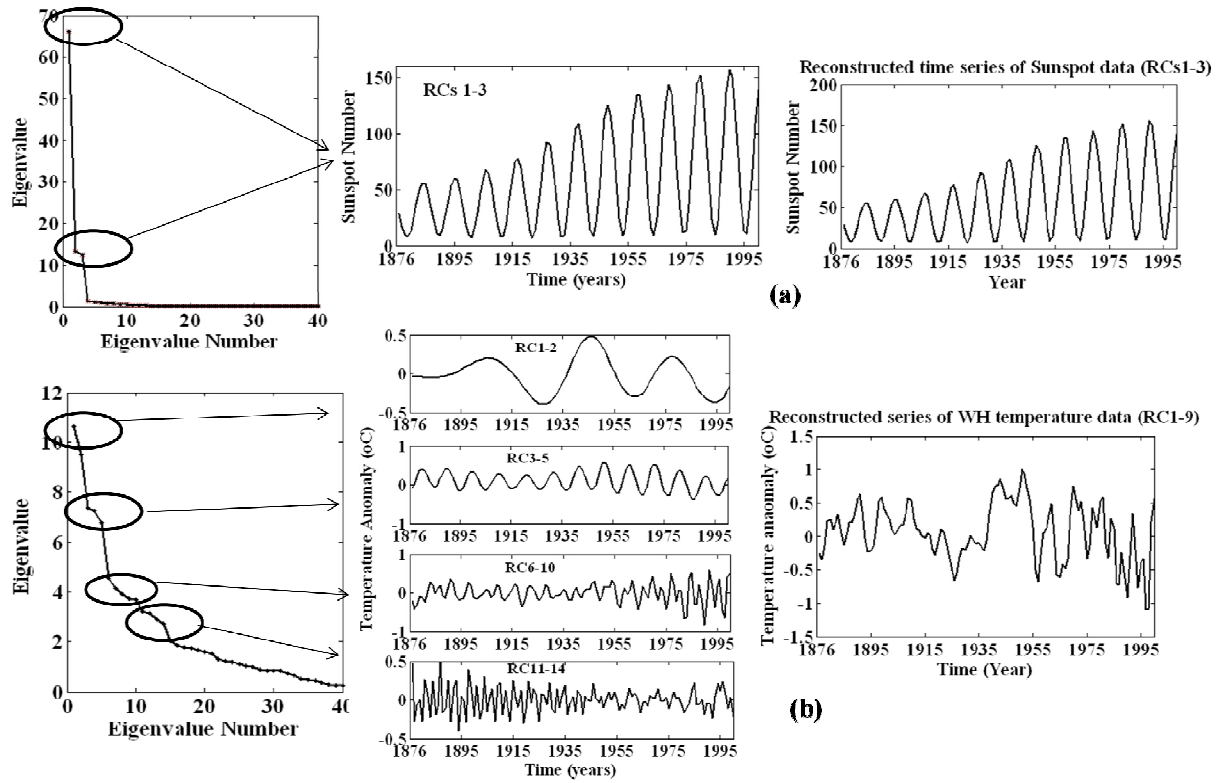
652

653



654

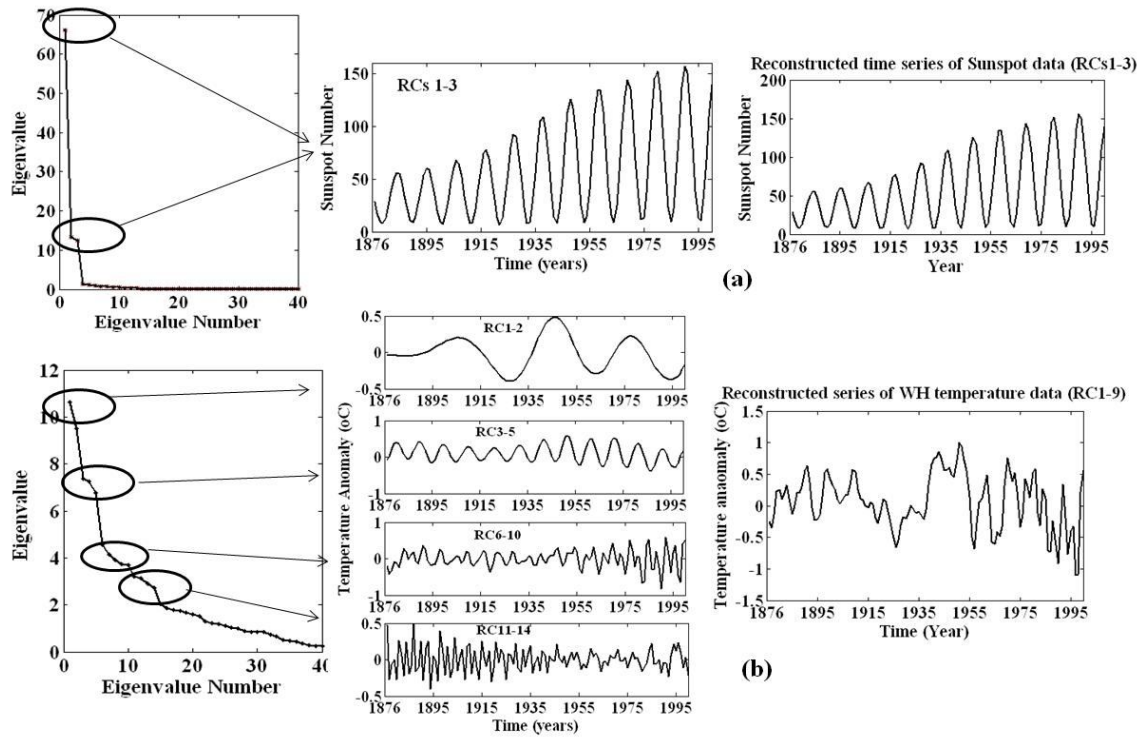
655 **Figure 5. Cross Wavelet spectrum between (a) Sunspot number-Western Himalayan data**
 656 **(b) Western Himalayan-Southern Oscillation Index (c) Sunspot number- Southern**
 657 **Oscillation Index and (d) Geomagnetic: aa indices-Western Himalayan data with cone of**
 658 **influence (lighter shade smooth curve) and black lines indicate significant power on 95%**
 659 **level compared to red noise based on AR(1) coefficient. The legend on right indicates the**
 660 **cross-wavelet power.**



661

662 **Figure 6. Singular spectra with its SSA decomposed components & its reconstructed time**
 663 **series for (a) Sunspot Number and (b) Western Himalaya temperature data.**

664

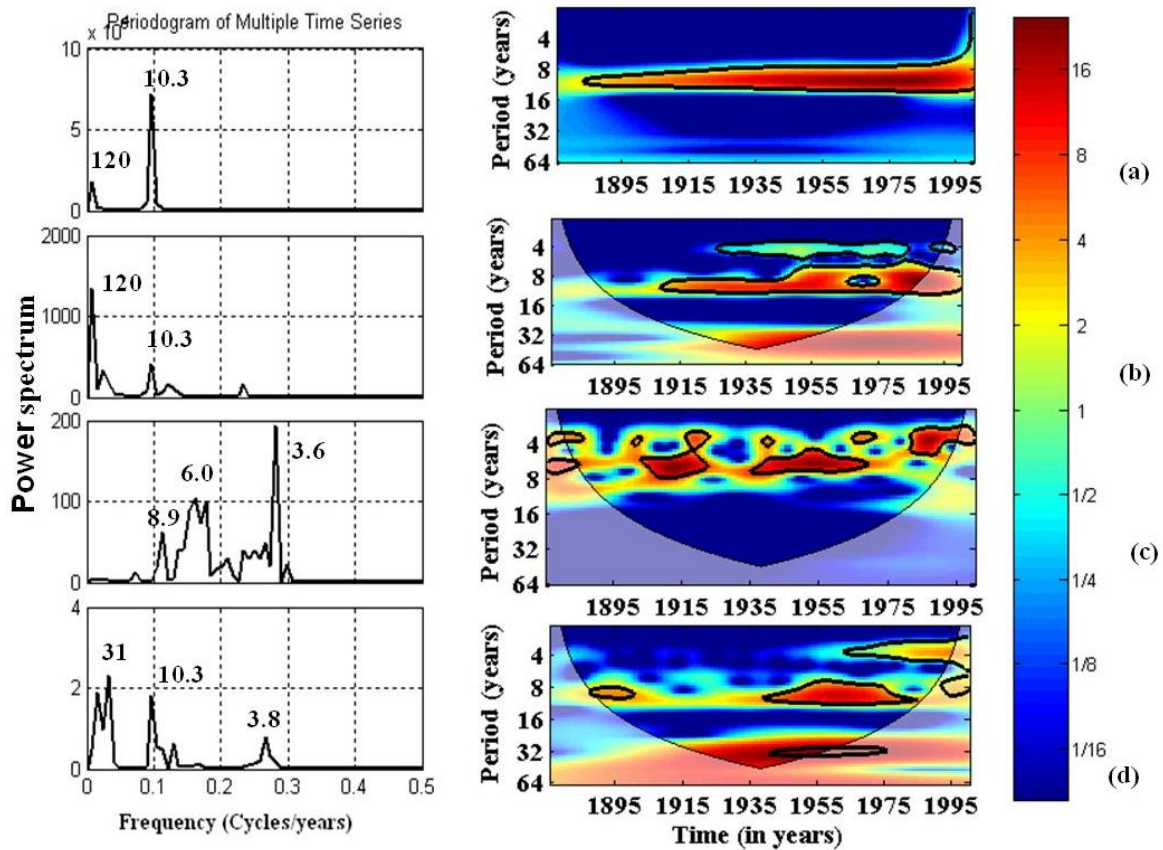


665

666

667

Figure 7. Singular spectra with its SSA decomposed components & its reconstructed time series for (c) SOI and (d) Geomagnetic activity (aa Indices).



668

669 **Figure 8. Power spectrum and Wavelet power spectrum of SSA reconstructed (a) Sunspot**
 670 **data (b) Geomagnetic Indices (aa index) (c) SOI index and (d) the Western Himalayas**
 671 **temperature data with cone of influence (lighter shade smooth curve) and black lines indicate**
 672 **significant power on 95% level compared to red noise based on AR(1) coefficient. The legend**
 673 **on right indicates the cross-wavelet power.**

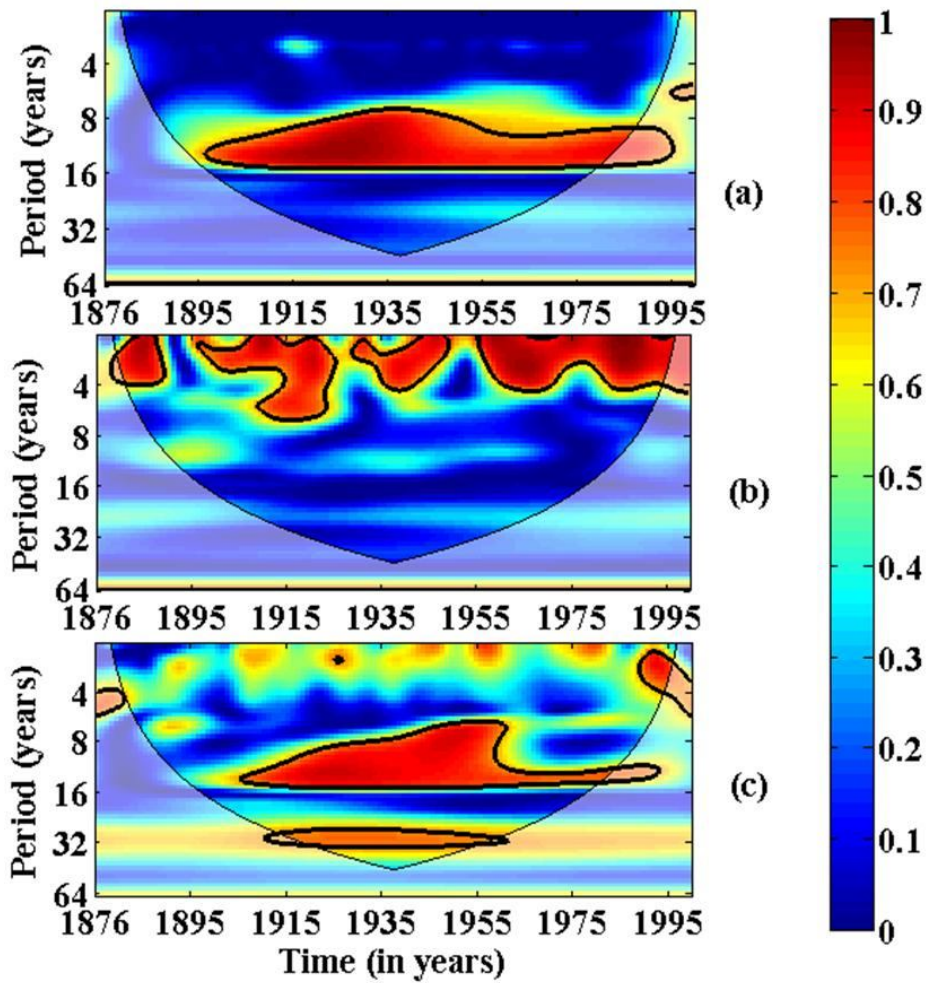
674

675

676

677

678



679

680 **Figure 9. Squared wavelet coherence plotted for the SSA reconstructed time series between**
 681 **(a) WH-SSN (b) WH-SOI and (c) WH-aa index with cone of influence (lighter shade smooth**
 682 **curve) and black lines indicate significant power on 95% level compared to red noise based on**
 683 **AR(1) coefficient.**

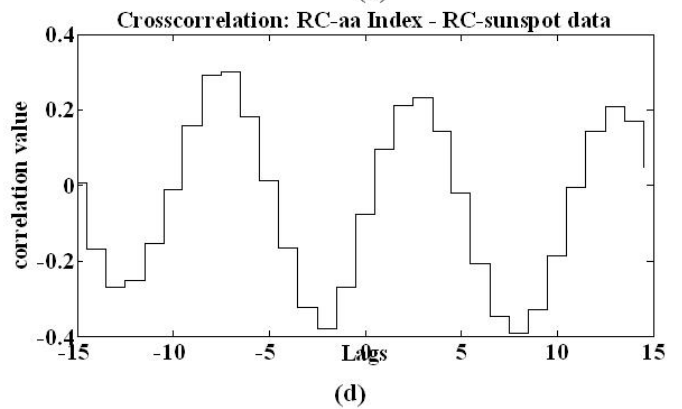
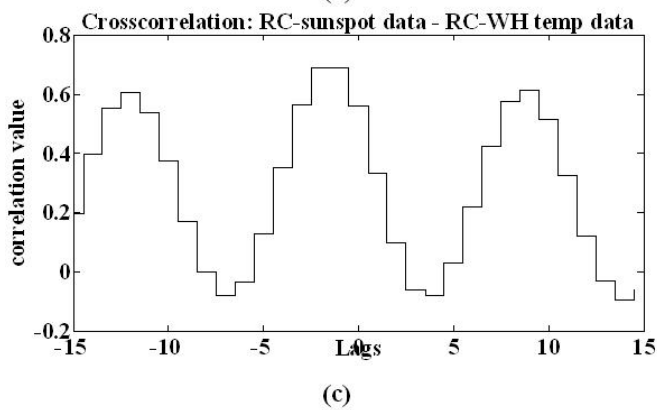
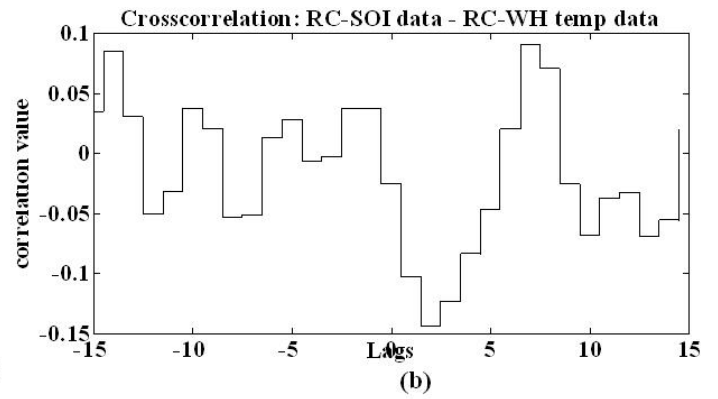
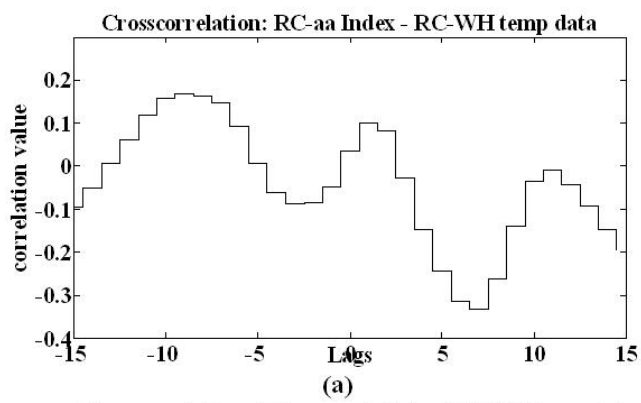
684

685

686

687

688



689

690 **Figure 10. Cross-correlation of SSA reconstructed time series of (a) aa Index-Western**
 691 **Himalayan (WH) temperature data; (b) SOI-WH temperature data; (c) sunspot -WH data and**
 692 **(d) aa Index-sunspot data.**

693

694

695